

Article

Effect of Citric Acid on MoO₃/Al₂O₃ Catalysts for Sulfur-Resistant Methanation

Dajun Meng, Baowei Wang *, Wenxia Yu, Weihang Wang, Zhenhua Li and Xinbin Ma *

Key Laboratory for Green Chemical Technology of Ministry of Education, School of Chemical Engineering and Technology, Tianjin University, Tianjin 300072, China; mdj02_17@163.com (D.M.); yuwenxia0917@163.com (W.Y.); wangwh@tju.edu.cn (W.W.); zhenhua@tju.edu.cn (Z.L.)

* Correspondence: wangbw@tju.edu.cn (B.W.); xbma@tju.edu.cn (X.M.);

Tel.: +86-13920159176 (B.W.); +86-13502069764 (X.M.)

Academic Editors: Benoît Louis, Qiang Wang and Marcelo Maciel Pereira

Received: 6 December 2016; Accepted: 26 April 2017; Published: 12 May 2017

Abstract: A series of MoO₃/Al₂O₃ catalysts with different amounts (molar ratio of CA/Mo = 0, 1, 1.5, and 2) of citric acid (CA) prepared by simultaneous impregnation were evaluated for sulfur-resistant methanation. Based on the evaluation results, catalytic activity increased accompanied with the rise of citric acid amount. Combine with the analysis of N₂-physisorption, XRD, H₂-TPR, XPS, and TEM, the catalyst saturated loading capacity improved, resulting in increasing dispersion of Mo species on Al₂O₃ surface clearly. According to H₂-TPR result, the Mo oxide precursors can be more easily sulfured when citric acid is added. Moreover, based on the Raman analysis, increasingly tetrahedrally coordinated Mo⁶⁺ species with high methanation performance are generated after citric acid treatment. These factors probably together accelerate MoO₃/Al₂O₃ catalytic activity growth for methanation.

Keywords: sulfur-resistant methanation; citric acid; dispersion; active Mo oxide precursor

1. Introduction

With the energy shortage and contamination crisis on the environment [1], the efficient and clean use of coal resources has become increasingly significant. The production of synthetic natural gas (SNG) from coal is an important method utilizing coal effectively [2]. Methanation is an essential process for SNG production. Traditionally, Ni-based catalyst can be used for a methanation reaction [3,4], but it is extremely sensitive to sulfur and only occurs as the molar ratio of H₂/CO is no less than 3:1.

Considering its good performance in water-gas shift (WGS) reactions [5], Mo-based catalysts can exhibit good methanation activity at relatively low H₂/CO. As a consequence, the chemical equation for sulfur-resistant methanation on Mo-based catalyst can be expressed in the following equation [6]. Moreover, the Mo-based catalysts resistance to sulfur poisoning has also been recognized [7–11].



Citric acid has been widely used as a chelating agent in hydrogenation reactions on Mo-based catalyst, and has been proven to be effective in increasing catalytic activity. Bergwerff et al. [12] reported that the agglomeration of Mo species can be removed by adding citric acid when the MoO₃ loading was beyond the saturated coverage of the catalyst. This suggested that citric acid could improve the dispersion of Mo species on the support surface efficiently. Furthermore, Wang et al. [10] found that citric acid could change the textural properties of catalysts and further increase the dispersion of active components. Similarly, Valencia et al. [13] and Peña et al. [14] also proved that citric acid was helpful in improving the Mo dispersion on support. Moreover, as one of the most important

chelating agents, citric acid could increase the sulfidation of Mo species for sulfided Mo/Al₂O₃ catalysts. Rinaldi et al. [15,16] reported that the addition of citric acid weakens the interaction of Mo species and Al₂O₃ support obviously, resulting in a significantly increasing sulfidation of the catalyst and improved catalytic performance for the hydrodesulfurization (HDS) of thiophene.

Obviously, citric acid performs a great function in Mo-based catalysts for hydrogenation reactions. Our previous study [17] has reported the structure of MoO₃/Al₂O₃ catalysts and their catalytic performance for sulfur-resistant methanation reactions. In this work, the role of citric acid in MoO₃/Al₂O₃ catalyst was studied. A series of MoO₃/Al₂O₃ catalysts with different amounts of citric acid were prepared by simultaneous impregnation, and the prepared catalysts were tested for sulfur-resistant methanation and characterized by N₂-physisorption, X-ray diffraction (XRD), H₂-temperature programmed reduction (H₂-TPR), transmission electron microscope (TEM), and Raman.

2. Results and Discussion

2.1. N₂-Physisorption

The N₂ adsorption–desorption isotherms of all CAMo/Al₂O₃ catalysts and Al₂O₃ support are shown in Figure 1. All samples showed typical and similar IV curves, with hysteresis loops according to the IUPAC classification system. Therefore, it can be concluded that the mesoporous structure presents all catalysts and support.

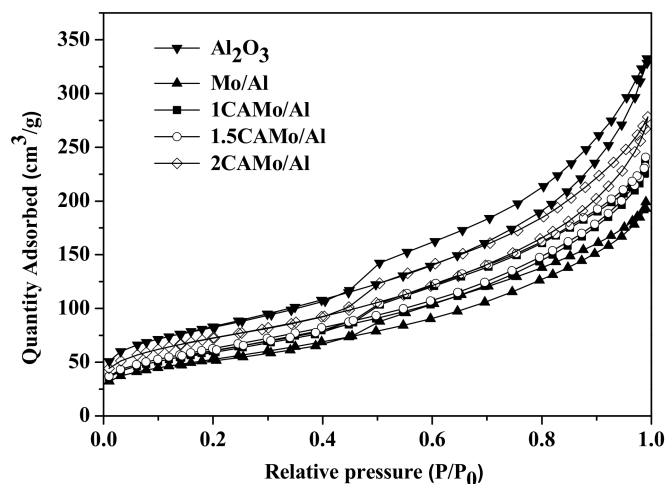


Figure 1. N₂ adsorption–desorption isotherms of CAMo/Al catalysts and Al₂O₃ support.

The N₂ physisorption results of CAMo/Al catalysts and Al₂O₃ support are listed in Table 1. After adding citric acid into catalysts, the Brunauer–Emmett–Teller (BET) surface area, the average pore volume, and the pore size of all catalyst samples are smaller than the Al₂O₃ support. Obviously, the impregnation of Mo may gather on the support and block the micropores of the catalysts. Therefore, the S_{BET} , the average pore volume, and the pore size of all catalyst samples become smaller than the Al₂O₃ support. The N₂ physisorption results of all CAMo/Al catalysts after the sulfidation are also listed in Table 1. Compared with the oxide catalysts, the sulfide catalysts possess a lower BET surface area and a higher pore size. With the increase in the CA/Mo ratio, the BET surface area and average pore volume of oxide catalysts and sulfide catalysts both increased gradually. Citric acid played an important role in modifying the texture properties of the catalysts. The change is attributed to the fact that the gas (CO₂ and water vapor), which is produced by the thermal decomposition of citric acid, can get through some holes inside the catalysts and block the agglomeration of MoO₃. Moreover, the pore size diameters are not influenced by the addition of citric acid. Figure 2 shows the pore size

distribution of all catalysts and Al₂O₃ support, indicating that an average pore diameter of 3–5 nm is found among them. The impregnation of Mo does not change the pore size distribution of the catalyst.

Based on the textural properties of the catalysts, the molybdenum could be dispersed better on the support surface modified by citric acid. This viewpoint will be also confirmed by the results of XRD, TEM, and TPR in later sections.

Table 1. Textural properties and Raman results of catalysts and Al₂O₃ support.

Samples	BET Surface Area (m ² /g)	Pore Size (nm)	Pore Volume (cm ³ /g)	S _t /S _o ¹
Mo/Al	190	6.1	0.3	0.08
1CAMo/Al	219	6.1	0.4	0.11
1.5CAMo/Al	228	6.2	0.4	0.12
2CAMo/Al	261	6.3	0.4	0.13
Al ₂ O ₃	298	6.5	0.5	/
Mo/Al-(AS) ²	158	7.0	0.3	/
1CAMo/Al-(AS)	162	7.0	0.3	/
1.5CAMo/Al-(AS)	170	6.9	0.4	/
2CAMo/Al-(AS)	186	7.6	0.4	/

¹ S_t: the peak area of tetrahedral Mo⁶⁺, S_o: the peak area of octahedral Mo⁶⁺, S_t/S_o: the area ratio of S_t/S_o;

² Catalyst-(AS): the catalyst samples after the sulfidation.

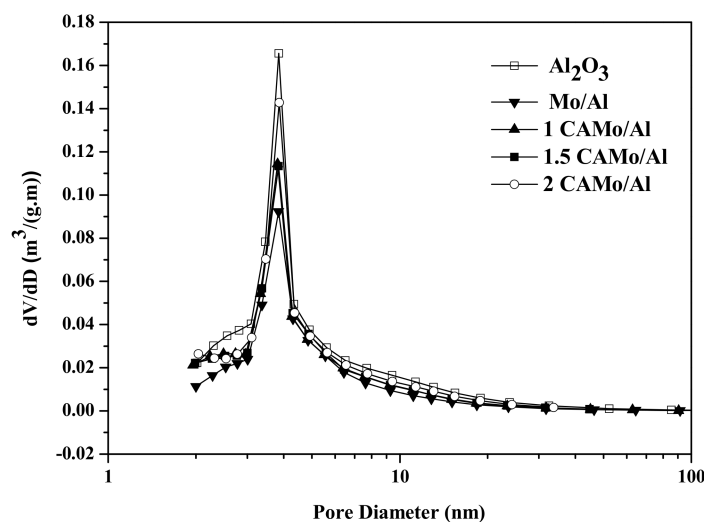


Figure 2. Pore size distribution of catalysts and support.

2.2. XRD Analysis

The XRD patterns of Al₂O₃ support and a series of CAMo/Al catalysts with different molar ratio of CA/Mo are shown in Figure 3. For all catalysts, the diffraction peaks $2\theta = 45.8^\circ$ and 67.1° are assigned to γ -Al₂O₃ (PDF-10-0425) [18]. The Mo/Al catalyst exhibits diffraction peaks at $2\theta = 23.4^\circ$ and 25.7° which are assigned to the crystalline MoO₃ phase [19], and other peaks at $2\theta = 20.7^\circ$, 22.0° , 23.4° and 25.7° are attributed to the Al₂(MoO₄)₃ phase. After the citric acid addition, the characteristic diffraction peaks of MoO₃ and Al₂(MoO₄)₃ disappeared. All CAMo/Al catalysts and Al₂O₃ support only exhibited typical diffraction peaks of γ -Al₂O₃.

Obviously, the lack of a crystalline MoO₃ peak indicates that MoO₃ is dispersed better as an amorphous form on the Al₂O₃ supports modified by citric acid. Otherwise, according to our previous study [17], the Al₂(MoO₄)₃ phase can be formed, as the MoO₃ loading exceeded the saturated monolayer coverage with calcination temperatures of 600 °C. Therefore, the disappearance of Al₂(MoO₄)₃ should be attributed to the change in the catalyst saturated monolayer coverage. Combined with the increase in BET surface area and the average pore volume from the N₂-physisorption results,

it can be concluded that the saturated loading capacity of the catalyst can be improved when citric acid is added.

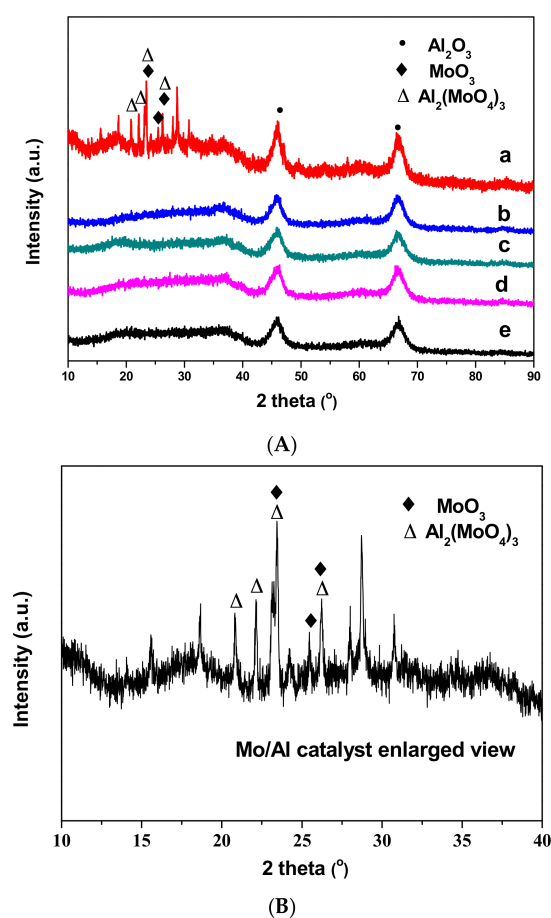


Figure 3. XRD patterns of catalysts and support: (a) Mo/Al; (b) 1CAMo/Al; (c) 1.5CAMo/Al; (d) 2CAMo/Al; (e) Al₂O₃. (A) XRD patterns of all samples; (B) The partial enlarged drawing of Mo/Al catalyst description.

2.3. H₂-TPR Analysis

The TPR profiles of the series of CAMo/Al catalysts, as well as Mo/Al catalyst, are shown in Figure 4. It can be seen that two main hydrogen consumption peaks around 430 and 840 °C were found in the profiles among them. According to Chary et al. [20], both tetrahedral and octahedral Mo⁶⁺ species were present when the Mo loading was not low. The interaction between tetrahedral Mo⁶⁺ and Al₂O₃ is stronger than the interaction between octahedral Mo⁶⁺ and Al₂O₃. The tetrahedral Mo⁶⁺ species are difficult to reduce due to the strong interaction with support. Therefore, the first peak at the low temperature region is attributed to the partial reduction of octahedral Mo⁶⁺ species from Mo⁶⁺ to Mo⁴⁺ and the reduction of small crystalline MoO₃ [21,22]. Meanwhile, the second peak at the high temperature region is assigned to the reduction of the tetrahedral Mo⁶⁺ species [23,24], and the further reduction of MoO₂ from Mo⁴⁺ to Mo⁰ [17].

As shown in Figure 4, the peaks in the low temperature region and the high temperature region both shifted to the left, significantly accompanied with the rise of citric acid amounts. On the one hand, the change in the peaks' positions implies that the reduction of different Mo species becomes easier when citric acid is added. It also means that the addition of citric acid can effectively weaken the interaction of Al₂O₃ support and Mo species. As a result, it is easier to achieve sulfidation of Mo oxide precursors to generate sulfide catalyst with high CO methanation activity.

On the other hand, the peak at the low temperature zone consists of the superposition of two hydrogen consumption peaks. Specifically, the first hydrogen consumption peak is assigned to the octahedral Mo species (300–500 °C), and the second hydrogen consumption peak is attributed to the reduction of small crystalline MoO₃ to MoO₂ (500–600 °C). Therefore, the crystalline MoO₃ species decrease and the amorphous Mo species increase when the reduction peak in the low-temperature region shifts to the lower temperature side. As certified by the previous XRD analysis, the crystalline and agglomerate MoO₃ can be removed when citric acid is added.

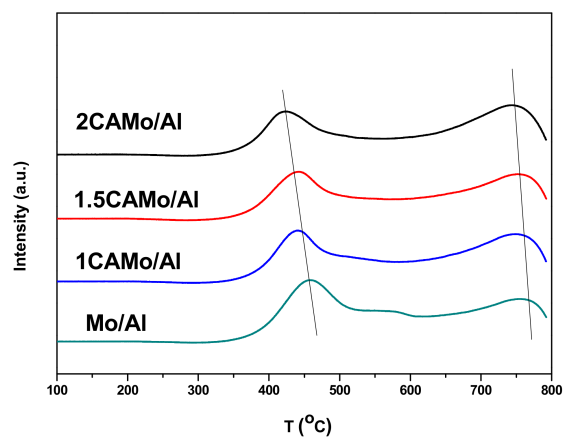


Figure 4. H₂-TPR profiles of catalysts.

2.4. TEM Analysis

Figure 5 shows the representative TEM images for Mo/Al and CAMo/Al catalysts with different molar ratios of CA/Mo. As shown in Figure 5a, the bulk MoO₃ species gathered on the surface of Al₂O₃. After the addition of citric acid into the precursors, the aggregation of MoO₃ is disappeared (see Figure 5b–d). Meanwhile, the needle-like Al₂O₃ can be clearly observed, suggesting that the Mo species dispersed better on the Al₂O₃ supports with the increase of citric acid content.

In order to explore the dispersion of Mo element in each catalyst, the mapping image of the catalysts has been observed. As shown in Figure 6, the yellow zone in the pictures stands for Mo; the black zone stands for other elements in the catalysts. In Figure 6a, the brightness of different yellow zones are not the same, and the distribution is unbalanced. However, in Figure 6b, the brightness and distribution of these yellow zones are totally different from those in Figure 6a. Therefore, the dispersion of Mo in the 2CAMo/Al catalyst is superior to that in the Mo/Al catalyst.

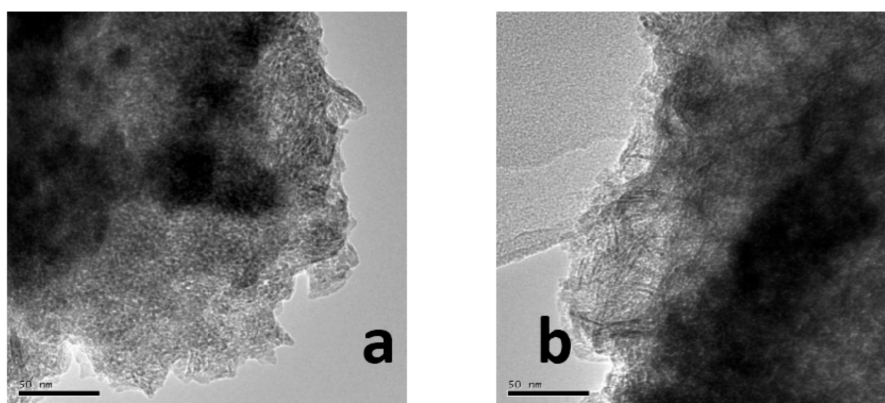


Figure 5. Cont.

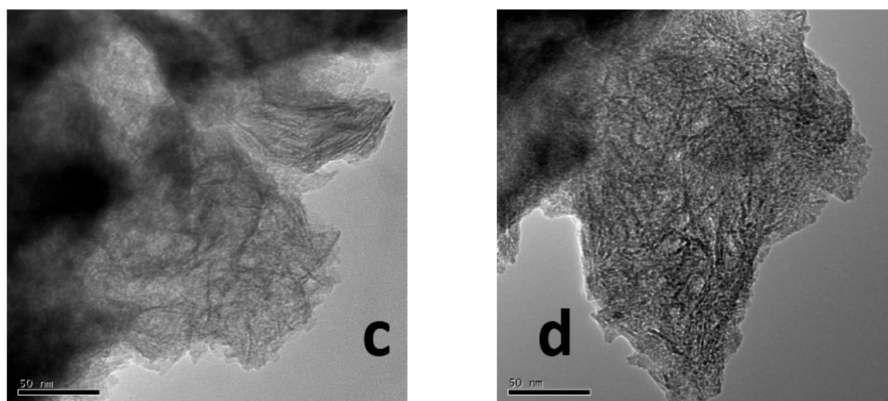


Figure 5. TEM images of catalysts: (a) Mo/Al; (b) 1CAMo/Al; (c) 1.5CAMo/Al; (d) 2CAMo/Al.

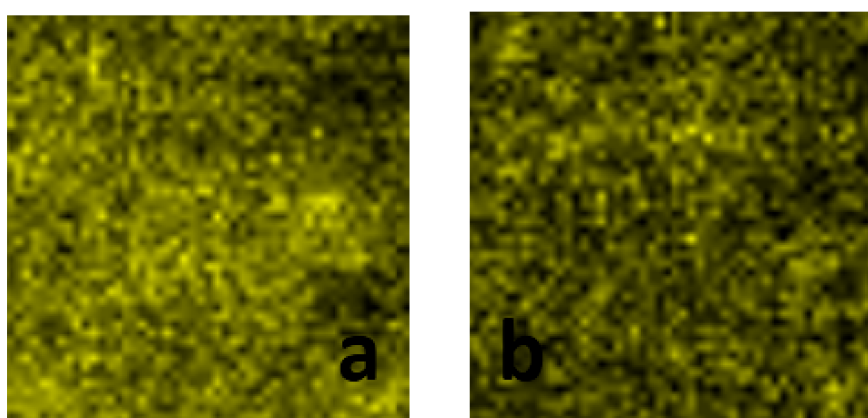


Figure 6. The Mo element of TEM mapping images for catalysts: (a) Mo/Al; (b) 2CAMo/Al.

To be summarized, based on the different characterization analysis above, citric acid performs a function in increasing the dispersion of Mo species on the support surface. As shown in Figure 3, the diffraction peaks of MoO_3 and $\text{Al}_2(\text{MoO}_4)_3$ appear in the curve of the Mo/Al catalyst sample. However, no diffraction peaks corresponding to the crystalline MoO_3 and $\text{Al}_2(\text{MoO}_4)_3$ were detected on any other CAMo/Al catalysts. Similarly, the H_2 -TPR profiles in Figure 4 also demonstrated that the crystalline MoO_3 decreases when citric acid content gradually increases. In fact, the results of N_2 -physisorption indicate that the disappearance of MoO_3 and $\text{Al}_2(\text{MoO}_4)_3$ is due to the change of catalyst textural properties. Based on the increase of the catalyst BET surface area, the saturated loading capacity of the catalyst is improved. Therefore, the MoO_3 can disperse better on the CAMo/Al catalyst than on the Mo/Al catalyst. Moreover, this can be directly observed in the mapping images of TEM.

2.5. Raman Analysis

To obtain a deeper understanding about the function of citric acid on modifying catalysts, the Mo/Al and CAMo/Al catalysts were characterized by Raman analysis. The characterization results of all catalyst samples are presented in Figure 7.

According to Figure 7, the detection range of the Raman band for all samples is from 200 to 1000 cm^{-1} . The sharpest Raman peak, observed around 954 cm^{-1} , can be assigned to the symmetric stretching vibration modes of the terminal $\text{Mo}=\text{O}$ bond, which is supposed to be an amorphous Mo^{6+} species in an octahedral environment [25]. Moreover, a relatively intense peak at 878 cm^{-1} and two weak peaks at 852 and 320 cm^{-1} are attributed to the $\text{Mo}-\text{O}-\text{Mo}$ asymmetric stretching and to the bending modes of the tetrahedrally coordinated Mo^{6+} species, respectively [26].

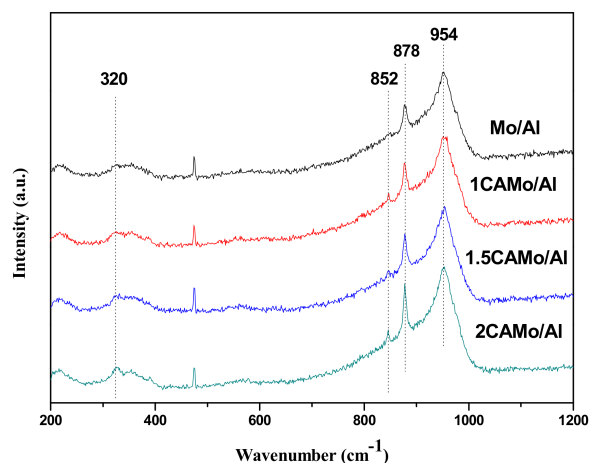


Figure 7. Raman spectra of catalysts.

Clearly, the peak intensity of tetrahedral and octahedral Mo^{6+} species significantly changed when citric acid was added. The area ratio (S_t/S_o) of the tetrahedral Mo^{6+} specie peak with respect to the octahedral Mo^{6+} specie peak can be used as a measure to detect the content of different Mo^{6+} species among samples. As listed in Table 1, there is an apparent increase about the value of S_t/S_o from 0.08 to 0.13 when the ratio of CA to Mo is from 0 to 2. It is indicated that the amount of tetrahedral Mo^{6+} species increases as citric acid content increased.

The addition of citric acid has an obvious effect on the change of the active catalytic precursor. In our previous study [17], the tetrahedrally coordinated Mo^{6+} was proven to be an active catalytic precursor for sulfur-resistant methanation. Based on the variation trend of S_t/S_o for different catalysts from the Raman result in Table 1, citric acid helps to increase the relative content of tetrahedral Mo^{6+} species in catalysts. Therefore, with the increase of tetrahedrally coordinated Mo^{6+} , the methanation activity is supposed to gradually improve. This trend is consistent with the results of the catalytic activity evaluation described in later section.

2.6. XPS Analysis

Figure 8 shows the distribution of S in different catalysts after sulfidation. As shown in Figure 8, the ratio of S species to Al species on the catalyst surface is steadily increased with citric acid amounts. Especially when the value of $n(\text{CA})/n(\text{Ce})$ is beyond 1, the growth rate of S/Al atomic ratio increases. Based on the XPS result, the addition of citric acid can increase the degree of sulfidation for the catalyst. Obviously, this conclusion is in agreement with the H_2 -TPR result.

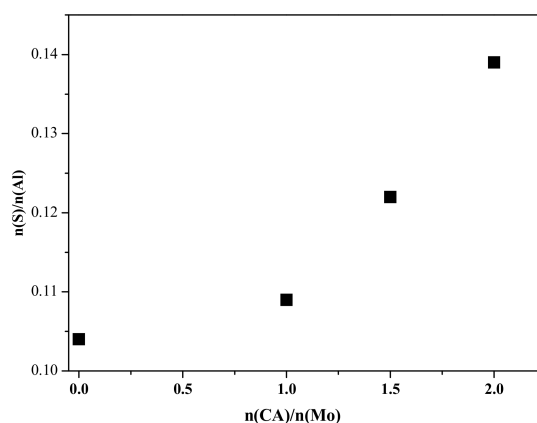


Figure 8. Elemental distribution of S in different catalysts after sulfidation.

2.7. Catalytic Activity Evaluation

The Mo/Al and a series of CAMo/Al catalysts were evaluated for CO methanation of syngas with a H₂/CO ratio of 1:1 and 0.27% H₂S. As shown in Figure 9, the CO conversion increased from 42% to 49% accompanied with the gradual rise of citric acid amounts. In addition, the hydrocarbon distribution of reaction products is listed in Table 2. Based on the data in Table 2, the selectivity of CH₄, which is the destination product for all catalysts, maintains a high value beyond 96% during reaction. The selectivity of C₂H₆ and C₃H₈ are only around 3% and 0.2%, respectively. It is clear that citric acid cannot affect the selectivity of products.

According to the experimental results, the addition of citric acid can improve the activity of Mo/Al catalysts for methanation. On the one hand, the results of XRD (Figure 3) and H₂-TPR (Figure 4) demonstrate that the inactive crystalline MoO₃ and Al₂(MoO₄)₃ decreased or even disappeared after using citric acid. On the other hand, Raman analysis reveals that the amount of tetrahedral Mo⁶⁺ species with high CO methanation activity increased. In addition, the H₂-TPR and XPS also show that citric acid can weaken the Mo–support interaction and increase the degree of sulfidation for the catalyst. These factors are all in favor of increasing the CO methanation activity of the Mo/Al catalyst.

Meanwhile, as for both 1.5CAMo/Al and 2CAMo/Al catalysts, their catalytic performance are enhanced slowly in the first 15 h of reaction, and then hold steady. As the amount of active Mo oxide precursor increased, a growing number of Mo–S active sites were formed from reactions with syngas (including H₂S) during this period.

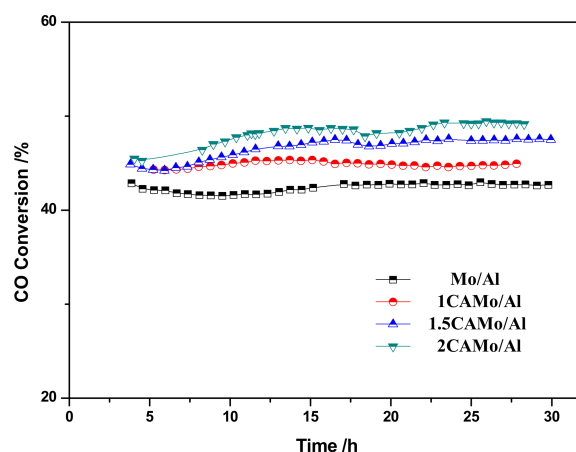


Figure 9. CO Conversion with time on stream on catalysts.

Table 2. Catalytic behavior of catalysts.

Catalyst	CO Conversion (%)	Selectivity to Hydrocarbon (%) (CO ₂ Free)		
		CH ₄	C ₂ H ₆	C ₃ H ₈
Mo/Al	42	96.9	3.0	0.1
1CAMo/Al	45	96.9	2.9	0.1
1.5CAMo/Al	47	96.3	3.5	0.2
2CAMo/Al	49	96.3	3.4	0.2

3. Materials and Methods

3.1. Catalyst Preparation

The commercial γ -Al₂O₃ powder was purchased from Yixing Qianye Non-metallic material Co. Ltd., Yixing, China, and the other reagents were purchased from Kemiou Chemical Reagent Co. Ltd., Tianjin, China.

All catalysts were prepared by simultaneous impregnating γ - Al_2O_3 powder was impregnated with the aqueous solutions of $(\text{NH}_4)_6\text{Mo}_7\text{O}_{24}\cdot 4\text{H}_2\text{O}$ and citric acid (CA). Then, the mixtures were continuously stirred at room temperature for 24 h, and subsequently dried at $120\text{ }^\circ\text{C}$ for 12 h. Finally, the samples were calcined at $600\text{ }^\circ\text{C}$ for 4 h at a heat rate of $5\text{ }^\circ\text{C}/\text{min}$. The MoO_3 content was fixed at 20 wt % with respect to Al_2O_3 for all catalysts. The catalysts are denoted as $x\text{CAMo}/\text{Al}$, where x represents the molar ratio of citric acid to Mo and ranges from 0 to 2. When the molar ratio of citric acid to Mo is 0, the sample is denoted as Mo/Al .

3.2. Catalyst Characterization

3.2.1. N_2 -Physisorption

N_2 -physisorption of the catalysts was performed at $-196\text{ }^\circ\text{C}$ with a Tristar 3000 apparatus (Micromeritics, Norcross, GA, USA). As a pretreatment of the N_2 physisorption analysis, each fresh sample should be degassed at $300\text{ }^\circ\text{C}$ for 4 h in vacuum.

3.2.2. XRD Analysis

The XRD was detected on a D/max-2500 X-ray diffractometer (Rigaku, Tokyo, Japan) with Ni-filtered $\text{Cu-K}\alpha$ radiation ($\lambda = 1.54056\text{ \AA}$). The angles of scanning were from 10° to 90° with a rate of $5\text{ }^\circ/\text{min}$. The XRD phases were identified by comparison with powder diffraction data from the Joint Committee on Powder Diffraction Standards (JCPDS).

3.2.3. H_2 -TPR Analysis

TPR profiles of the prepared samples were obtained by 2910 Automatic chemical adsorption instrument (Micromeritics). Before each TPR measurement, approximately 200 mg of catalyst was flushed with 99.999% argon at $200\text{ }^\circ\text{C}$ for 40 min to remove traces of water. A gas mixture of 10% (v/v) of hydrogen in argon was used at a flow rate of 30 mL/min, and the temperature was increased at a heating rate of $10\text{ }^\circ\text{C}/\text{min}$ from 60 to $1000\text{ }^\circ\text{C}$.

3.2.4. TEM Analysis

The morphology and structure of the catalyst samples were observed by a Tecnai G2 F20 (200 kV) transmission electron microscope (TEM) (FEI, Eindhoven, The Netherlands), with a high resolution of 0.15 nm/200 kV. The catalyst samples were prepared via ultrasonic dispersion in ethanol, and a drop of the suspension was then put on a lacey carbon film supported on a Cu grid.

3.2.5. Raman Analysis

The Raman spectra of Mo/Al and samples with a citric acid addition were obtained using an InVia-Reflex (Renishaw, Wotton-under-Edge, Gloucestershire, UK) laser Raman spectrometer with a highly sensitive system of integrated research grade microscopes. The 532 nm line of an Ar^+ laser was used.

3.2.6. X-ray Photoelectron Spectroscopy Analysis

X-ray photoelectron spectroscopy was analyzed using Perkin Elmer PHI-1600 XPS spectrometer (PerkinElmer, Waltham, MA, USA) with $\text{Mg K}\alpha$ X-ray radiation. The binding energy of C 1s at 284.6 eV was a reference to the binding energies.

3.3. Catalytic Activity Evaluation

The evaluation of sulfur-resistant methanation activity was carried out in a continuous-flow fixed-bed reactor (inner diameter: 12 mm; length: 700 mm) with a gas chromatograph equipped with a thermal conductivity detector and a hydrogen flame ionization detector. The loading quantity was

3 mL of catalyst for each experiment. The catalyst (3 mL) was sulfurized under a gas mixture of 3.0 vol % H₂S/H₂ at 400 °C for 4 h before the catalytic activity test. The activity test conditions were as follows: syngas (H₂/CO = 1.0) containing 0.27 vol % H₂S and 10 vol % N₂, a gas hourly space velocity of 5000 h⁻¹, at 550 °C and at 3 MPa.

The CO conversion and selectivity to hydrocarbons were calculated by using the following expressions:

$$X_{\text{CO}} = \frac{n(\text{CO})_{\text{in}} - n(\text{CO})_{\text{out}}}{n(\text{CO})_{\text{in}}} \times 100\% \quad (2)$$

$$S_{\text{CH}_4} = \frac{n(\text{CH}_4)_{\text{out}}}{n(\text{CH}_4)_{\text{out}} + n(\text{C}_2\text{H}_6)_{\text{out}} + n(\text{C}_3\text{H}_8)_{\text{out}}} \times 100\% \quad (3)$$

$$S_{\text{C}_2\text{H}_6} = \frac{n(\text{C}_2\text{H}_6)_{\text{out}}}{n(\text{CH}_4)_{\text{out}} + n(\text{C}_2\text{H}_6)_{\text{out}} + n(\text{C}_3\text{H}_8)_{\text{out}}} \times 100\% \quad (4)$$

$$S_{\text{C}_3\text{H}_8} = \frac{n(\text{C}_3\text{H}_8)_{\text{out}}}{n(\text{CH}_4)_{\text{out}} + n(\text{C}_2\text{H}_6)_{\text{out}} + n(\text{C}_3\text{H}_8)_{\text{out}}} \times 100\% \quad (5)$$

4. Conclusions

In the present study, a series of CAMo/Al catalysts prepared by simultaneous impregnation were tested for sulfur-resistant methanation. The activity of the CAMo/Al catalysts enhanced with the increase in citric acid content. Based on the characterization analysis, the following conclusions can be drawn. First, the addition of citric acid can change the textural properties of a catalyst and improves the dispersion for all kinds of Mo species on catalyst surfaces. Second, it can translate crystalline MoO₃ and Al₂(MoO₄)₃ into unformed Mo species, with relatively high catalytic activity. Moreover, the interaction of Al₂O₃ support with Mo species was gradually weakened when different amounts of citric acid were added. Therefore, MoO₃ is more easily sulfured to MoS₂, with highly catalytic activity in H₂/H₂S. In addition, the more tetrahedrally coordinated Mo⁶⁺ with high methanation activity can be formed using citric acid in this way.

Acknowledgments: Financial support from the National High Technology Research and Development Program of China (863 Project) (2015AA050504) is gratefully acknowledged.

Author Contributions: Baowei Wang and Xinbin Ma conceived and designed the experiments; Dajun Meng and Wenxia Yu performed the experiments; Baowei Wang and Dajun Meng analyzed the data; Zhenhua Li and Weihang Wang contributed reagents/materials/analysis tools; Dajun Meng wrote the paper.

Conflicts of Interest: The authors declare no conflict of interest.

References

1. Kustov, A.L.; Frey, A.M.; Larsen, K.E.; Johannessen, T.; Nørskov, J.K.; Christensen, C.H. CO methanation over supported bimetallic Ni-Fe catalysts: From computational studies towards catalyst optimization. *Appl. Catal. A* **2007**, *320*, 98–104. [[CrossRef](#)]
2. Kopyscinski, J.; Schildhauer, T.J.; Biollaz, S.M.A. Production of synthetic natural gas (SNG) from coal and dry biomass—A technology review from 1950 to 2009. *Fuel* **2010**, *89*, 1763–1783. [[CrossRef](#)]
3. Wang, Y.; Wu, R.; Zhao, Y. Effect of ZrO₂ promoter on structure and catalytic activity of the Ni/SiO₂ catalyst for CO methanation in hydrogen-rich gases. *Catal. Today* **2010**, *158*, 470–474. [[CrossRef](#)]
4. Li, H.; Ren, J.; Qin, X.; Qin, Z.; Lin, J.; Li, Z. Ni/SBA-15 catalysts for co methanation: Effects of V, Ce, and Zr promoters. *RSC Adv.* **2015**, *5*, 96504–96517. [[CrossRef](#)]
5. Sasaki, T.; Suzuki, T. Sulfide molybdenum catalysts for water-gas shift reaction: Influence of the kind of promoters and supports to generate MoS₂. *Appl. Catal. A* **2014**, *484*, 79–83. [[CrossRef](#)]
6. Jiang, M.; Wang, B.; Lv, J.; Wang, H.; Li, Z.; Ma, X.; Qin, S.; Sun, Q. Effect of sulfidation temperature on the catalytic activity of MoO₃/CeO₂-Al₂O₃ toward sulfur-resistant methanation. *Appl. Catal. A* **2013**, *466*, 224–232. [[CrossRef](#)]

7. Farag, H. Effect of sulfidation temperatures on the bulk structures of various molybdenum precursors. *Energy Fuels* **2002**, *16*, 944–950. [[CrossRef](#)]
8. Jalowiecki-Duhamel, L.; Grimblot, J.; Bonnelle, J.P. Effect of Mo loading of MoS₂/γ-Al₂O₃ on diene hydrogenation: Evidence of an “elementary ensemble” site. *J. Catal.* **1991**, *129*, 511–518. [[CrossRef](#)]
9. Frank, A.J.; Dick, H.A.; Goral, J.; Nelson, A.J.; Grätzel, M. MoS₂-catalyzed methanation of CO with H₂S. *J. Catal.* **1990**, *126*, 674–676. [[CrossRef](#)]
10. Wang, R.; Smith, K.J. Hydrodesulfurization of 4,6-dimethyldibenzothiophene over high surface area metal phosphides. *Appl. Catal. A* **2009**, *361*, 18–25. [[CrossRef](#)]
11. Kim, M.Y.; Ha, S.B.; Dong, J.K.; Byun, C.; Park, E.D. CO methanation over supported Mo catalysts in the presence of H₂S. *Catal. Commun.* **2013**, *35*, 68–71. [[CrossRef](#)]
12. Bergwerff, J.A.; Jansen, M.; Leliveld, B.G.; Visser, T.; Jong, K.P.D.; Weckhuysen, B.M. Influence of the preparation method on the hydrotreating activity of MoS₂/Al₂O₃ extrudates: A Raman microspectroscopy study on the genesis of the active phase. *J. Catal.* **2006**, *243*, 292–302. [[CrossRef](#)]
13. Valencia, D.; Klimova, T. Citric acid loading for MoS₂-based catalysts supported on SBA-15. New catalytic materials with high hydrogenolysis ability in hydrodesulfurization. *Appl. Catal. B* **2013**, *129*, 137–145. [[CrossRef](#)]
14. Peña, L.; Valencia, D.; Klimova, T. CoMo/SBA-15 catalysts prepared with edta and citric acid and their performance in hydrodesulfurization of dibenzothiophene. *Appl. Catal. B* **2014**, *147*, 879–887. [[CrossRef](#)]
15. Rinaldi, N.; Kubota, T.; Okamoto, Y. Effect of citric acid addition on the hydrodesulfurization activity of MoO₃/Al₂O₃ catalysts. *Appl. Catal. A* **2010**, *374*, 228–236. [[CrossRef](#)]
16. Rinaldi, N.; Kubota, T.; Okamoto, Y. Effect of citric acid addition on Co–Mo/B₂O₃/Al₂O₃ catalysts prepared by a post-treatment method. *Ind. Eng. Chem. Res.* **2009**, *48*, 10414–10424. [[CrossRef](#)]
17. Wang, B.; Ding, G.; Shang, Y.; Lv, J.; Wang, H.; Wang, E.; Li, Z.; Ma, X.; Qin, S.; Sun, Q. Effects of MoO₃ loading and calcination temperature on the activity of the sulphur-resistant methanation catalyst MoO₃/γ-Al₂O₃. *Appl. Catal. A* **2012**, *431–432*, 144–150. [[CrossRef](#)]
18. Suresh, R.; Ponnuswamy, V.; Mariappan, R. Effect of annealing temperature on the microstructural, optical and electrical properties of CeO₂ nanoparticles by chemical precipitation method. *Appl. Surf. Sci.* **2013**, *273*, 457–464. [[CrossRef](#)]
19. Zhang, Y.; Han, W.; Long, X.; Nie, H. Redispersion effects of citric acid on CoMo/γ-Al₂O₃ hydrodesulfurization catalysts. *Catal. Commun.* **2016**, *82*, 20–23. [[CrossRef](#)]
20. Chary, K.V.R.; Reddy, K.R.; Kishan, G.; Niemantsverdriet, J.W.; Mestl, G. Structure and catalytic properties of molybdenum oxide catalysts supported on zirconia. *J. Catal.* **2004**, *226*, 283–291. [[CrossRef](#)]
21. Scheffer, B.; Molhoek, P.; Moulijn, J.A. Temperature-programmed reduction of NiO WO₃/Al₂O₃ hydrodesulphurization catalysts. *Appl. Catal.* **1989**, *46*, 11–30. [[CrossRef](#)]
22. Srinivasan, T.K.K.; Mestl, G. Raman spectroscopy of monolayer-type catalysts: Supported molybdenum oxides. *Catal. Rev.* **1998**, *40*, 451–570.
23. Aberuagba, F.; Kumar, M.; Muralidhar, G.; Sharma, L.D. Characterization of Al₂O₃-ZrO₂ mixed oxide supported Mo hydrotreating catalyst. *Pet. Sci. Technol.* **2004**, *22*, 1287–1298. [[CrossRef](#)]
24. Maity, S.K.; Rana, M.S.; Srinivas, B.N.; Bej, S.K.; Dhar, G.M.; Rao, T.S.R.P. Characterization and evaluation of ZrO₂ supported hydrotreating catalysts. *J. Mol. Catal. A* **2000**, *153*, 121–127. [[CrossRef](#)]
25. Dufresne, P.; Payen, E.; Grimblot, J.; Bonnelle, J.P. Study of nickel-molybdenum-γ-aluminum oxide catalysts by X-ray photoelectron and Raman spectroscopy. Comparison with cobalt-molybdenum-γ-aluminum oxide catalysts. *J. Phys. Chem.* **1981**, *85*, 2344–2351. [[CrossRef](#)]
26. Plazenet, G.; Payen, E.; Lynch, J.; Rebours, B. Study by EXAFS, Raman, and NMR spectroscopies of the genesis of oxidic precursors of zeolite-supported HDS catalysts. *J. Phys. Chem. B* **2002**, *106*, 7013–7028. [[CrossRef](#)]

